IFASD 2015
International Forum on Aeroelasticity and Structural Dynamics
June 28 — July 02, 2015 ▲ Saint Petersburg, Russia

Time resolved PIV measurements of a hybrid morphing NACA4412 airfoil

Johannes Scheller[1,2], Karl-Joseph Rizzo[1], Gurvan Jodin[1,2], Eric Duhayon[1], Jean-Francois Rouchon[1], Giles Harran[2] and Marianna Braza[2]

[1]*Laboratoire Plasma et Conversion d'Energie, UMR CNRS-INPT-UPS N° 5213 , 2 Rue Charles Camichel , F-31071 Toulouse, France*
first.last@laplace.univ-tlse.fr

[2]*Institut de Mécanique des Fluides de Toulouse, UMR CNRS-INPT-UPS N° 5502, Alleé du Prof.Camille Soula, F-31400 Toulouse, France*
first.last@imft.fr

Keywords: Morphing, Turbulence, Aerodynamics, Shear layer, Time-resolved PIV

Abstract: Particle image velocimetry (PIV) measurements are conducted at the trailing edge of a piezoelectric actuated airfoil in order to investigate the physical effect on the flow via high-frequency low-amplitude actuation. Furthermore the effects of large-amplitude low frequency actuation modifying the airfoil camber are investigated using aerodynamic force measurements. A statistical analysis reveals the reduction of the Reynolds stress tensor components with increasing actuation frequency up to a frequency of 60 Hz. The modification of the airfoil camber allows real-time control of the desired lift. The feasibility of the designed hybrid morphing mechanism under aerodynamic loads at a Reynolds number of $218,000$ was shown for both the large amplitude and the high frequent actuation.

1 Introduction

Aerodynamic performance optimization using deformable structures are subject of much interest in the aerospace domain. Advances made in the domain of smart-materials have further intensified this interest [16]. The Electro-active morphing for micro-air-vehicles (EMMAV) research program, which was created as part of the French foundation of «Sciences et Technologies pour l'Aéronautique et l'Espace»'s effort to develop micro- and nano-air-vehicles and is composed of three French laboratories (IMFT, LAPLACE, ISAE), aims at optimizing the performance of micro-air-vehicles in realistic environments via electro-active morphing. To this end a hybrid NACA 4412 prototype was developed. The prototype, was selected to be displayed in the Royal Society annual Exhibition (1-6 July 2014). It is capable of both low frequent large amplitude actuation achieved using shape-memory alloys (SMAs) and high frequent small amplitude actuation via macro fiber composites (MFCs). The large amplitude actuation is primarily targeting the modification of the airfoil camber in order to optimize its shape and control the flight. The high frequency actuation achieved using MFC actuators intends to modify the aeroelastic coupling coefficient inducing both noise and drag.

Previous studies on SMA actuators activated using the Joule effect have already shown the capacity of the material to provide large deformations of the airfoil. Barbarino et al. [1] conducted a numerical investigation regarding the chordwise bending capacity of SMA actuated airfoils as well as the effect of the actuation on the lift and drag coefficients. Manzo [14] applied a SMA based pully mechanism in order to induce a spanwise deformation. He executed

wind-tunnel experiments and showed the deformation capacity of the SMA actuation under aerodynamic loads. The trailing edge dynamics of the deformation of an SMA actuated flat plate have been investigated by Deri et al. [8]. Chinaud et al. [7] showed the partial validity of the quasi-static hypothesis of the SMA actuation using time-resolved particle image velocimetry (TRPIV) measurements.

Similarily piezoelectric actuation has also been studied in the literature. Bilgen et al. [4] and Bilgen and Friswell [3] studied the use of MFCs for chordwise deformations on both tapered and 2D airfoils. Similar concepts have also been studied by Ohanian III et al. [17] and Bilgen and Friswell [3] showing the feasability of piezoelectrically actuated control surfaces for micro air vehicless (MAVs). Ohanian III et al. [17] developed a flexible fiberglass extension in order to achieve the desired airfoil shape and executed windtunnel test showing the actuation voltage dependence of the lift and drag coefficients. Whereas the previously described concepts primarily focus on the quasi-static shape control in order to control the flight and modify the airfoils lift/drag characteristics the effect of high-frequency oscillation on the detachment has been investigated by Munday and Jacob [15], who showed the capacity of thunder actuated oscillating cambers to delay detachment . Using piezoceramic actuators Orazi et al. [18] showed the influence on the flow of vibrating bimorphs on the example of a cylinder. Similar results have been obtained by [21] on a NACA0012 airfoil actuated via piezoceramic stack actuators inducing a deformation of a hinged trailing-edge flap.

Based on these results, the present study will investigate both the macroscopic and microscopic effects on the flow using a hybrid actuation system combining both the low-frequent high-amplitude SMA actuation as well as the high-frequent low-amplitude MFC actuation. The trailing edge dynamics are studied using time-resolved Particle Image Velocimetry measurements executed using a Phantom v1210 high speed camera at an acquisition frequency of $6\,\mathrm{kHz}$. The macroscopic effects are investigated using an aerodynamic balance as well as a pressure measurements conducted at the trailing edge of the hybrid airfoil.

The goals of this experiment are twofold: in a first step the effects of the actuation on the different velocity components is analyzed and in a second step this analysis will be used in order to optimize the flow over the airfoil prototype in order to reduce the aeroelastic coupling effect and optimize the shape of the airfoil in function of the current mission profile. To achieve this goal the MFCs were actuated at different frequencies ($30\,\mathrm{Hz}$, $60\,\mathrm{Hz}$ and $90\,\mathrm{Hz}$) both with and without SMA actuation. Hence, the effect of the trailing-edge vibration was studied both in a static configuration as well as during the induced camber change. The Reynolds number was fixed at 218.000 which corresponds to low velocities of an aircraft during take-off and landing. The measurements were conducted behind the trailing edge of the 10° inclined airfoil. The actuation effects on the trailing-edge instabilities will be discussed.

To the authors knowledge there are no studies in the state of the art performing a detailed experimental analysis in wind tunnel of a hybrid (SMA and piezoelectric) morphing wing. Previous studies focused primarly on the design and performance of the actuator and/or the macroscopic parameters such as lift and drag coefficients [5, 11]. This article will therefore focus both on studying the effect of the high-frequent piezoelectric actuation embedded at the trailing edge of a NACA4412 prototype and lower frequent large amplitude actuation using SMAs. Results indicate the capacity of the prototype NACA4412 airfoil to not only act on the lift but also to influence the Reynolds stress tensors via the high-frequent low amplitude MFC actuators.

This work is developed as follows: in a first part we recall the fundamental properties of both piezoelectric materials and SMAs as well as the developed actuation mechanisms for the prototype airfoil of $42.5\,\mathrm{cm}$ chord length. Subsequently the experimental set-up in the wind tunnel S4 of IMFT is described. Section 3 describes the experimental setup. The obtained

results of the particle image velocimetry (PIV), lift and pressure measurements are described in Section 4. Finally the obtained results will be summarized and perspectives for future work are shown.

2 Actuation mechanism

2 Piezoelectric material properties

Jacques and Pierre Curie discovered in 1880 that certain types of materials became electrically polarized when subjected to a mechanical force. This effect is today known as the direct piezoelectric effect and exploited in a variety of sensor and energy harvesting applications. The inverse effect, the deformation of the material when an electric field is applied, is used in different actuators from image stabelizers in cameras to accelerometers and elements for vibration control [12]. Piezoelectric materials are defined by an electro-mechanical coupling which can be described by the following equations:

$$\{S\} = [s^E] \cdot \{T\} + [d] \cdot \{E\} \tag{1}$$

$$\{D\} = [d] \cdot \{T\} + [\epsilon^T] \cdot \{E\} \tag{2}$$

where $\{S\}$ is the strain vector, $[s^E]$ is the compliance matrix, $\{T\}$ is the stress vector, $[d]$ is the matrix of piezoelectric constants, $\{D\}$ is the dielectric displacement vector, $[\epsilon^T]$ is the permittivity matrix and $\{E\}$ is the electric field vector.

In a previous study [21], piezoelectric stack actuators were integrated in a PUSH–PUSH lever mechanism to deform the rigid trailing edge of a NACA0012 airfoil. This first study has shown that actuation above 60 Hz with a limited amplitude has a significant effect on the shear layer.

To enhance this concept we are proposing a new architecture replacing piezoelectric stacks by MFCs. As in piezoelectric stacks the base material is a piezoelectric ceramic. Instead of a massive structure MFCs are an alignment of encapsulated fibers exploiting the significantly larger d_{33} mode of actuation. The fiber organisation is shown schematically in Figure 1. This structure represent an evolution of the active fiber composites (AFCs) originally developed at NASA Langely Research Center [22, 23]. MFCs combine piezoelectric fibers with interdigitated electrodes (IDEs) but the use of a uniform rectangular cross section fibers maximizes the electrode contact and furthermore facilitated the fabrication and integration of the actuator. The comercially available MFCs based on the developments by NASA are capable of strains up to 2000 ppm and blocking forces between 28 N and 1 kN for voltages between -500 V and 1500 V.

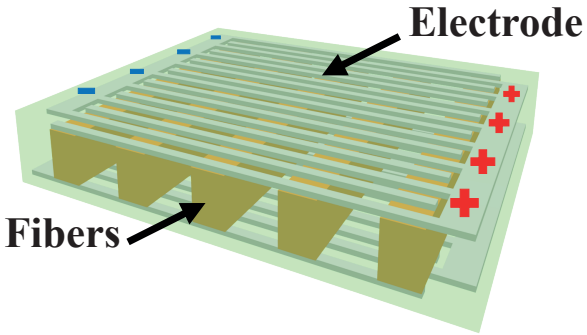

Figure 1: Fibers and electrodes organization in the MFC

2 Shape memory alloys

SMAs are defined by a thermo-mechanical coupling. Actuators based on SMA technologies generally modify the shape of a structure by changing the temperature of the material [13]. This kind of material is generally composed of a metallic alloy. In this paper the chosen material is NITINOL which is an alloy of nickel and titanium. This kind of SMA is well described in the literature [19, 2].

The shape modification of SMAs is due to a change in the crystalline phase induced by a variation of the material's temperature. One can distinguish between two different crystalline phases. The first one observed at low temperature is called the Martensitic phase. The second phase, called Austenite, is obtained upon heating of the material [9]. The macroscopic deformations are due to the break of the high symmetry level in the initial crystalline phase. The phase change is defined as a reversible non-instantaneous process. SMAs are characterized by a variety of properties such as super-elasticity during the phase change, the shape memory effect, etc.. However, one of the most important properties of SMAs is the hysteresis observed between the Martensite-Austenite transformation. Figure 2b shows the typical hysteresis curve observed for SMAs at different temperatures. The shape-memory effect (SME) is illustrated in Figure 2a showing the contraction of a nickel and titanium (NITI) wire ($\varnothing 1\,\mathrm{mm}$) under constant mechanical load upon temperature increase.

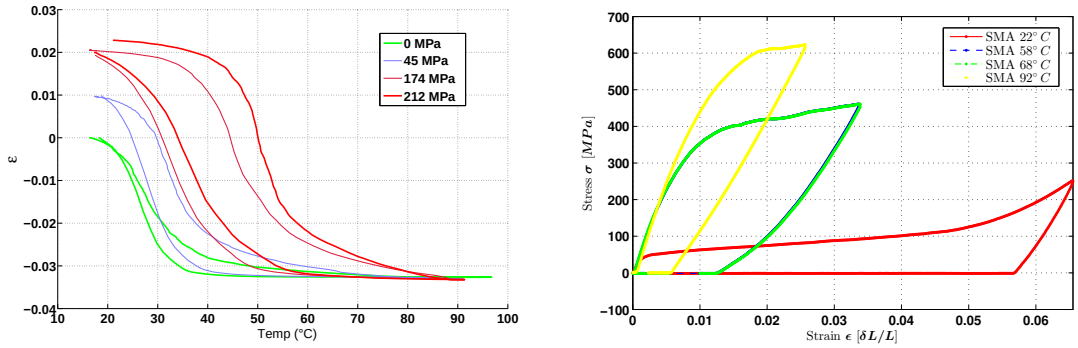

(a) ϵ Vs T° under constant stress

(b) σ Vs ϵ under constant temperature

Figure 2: SMA behaviour

Amongst all the mechanical properties of SMAs this work focuses on the shape memory effect as a means for actuation. By exploiting this material property the maximum deformation of a NITI wire is $\approx 8\%$ at constant stress. However for actuation purposes, the aforementioned hysteresis phenomenon has to be taken into account in order to precisely control the displacement.

2 Implementation

This article proposes a hybridization of MFC and SMA actuators in order to achieve both large displacement at low frequencies and small displacement at high frequencies. The integrated structure is shown in Figure 3.

As previously mentioned, MFCs allow for an easier integration compared to piezoelectric stack actuators. The used MFC actuated bimorph structures have a substrate thickness of $0.3\,\mathrm{mm}$. This configuration, shown in Figure 4a allows to cover $0\,\mathrm{Hz}$ to $120\,\mathrm{Hz}$ at +/-2mm of magnitude . The frequency response of the designed bimorphs is presented in Figure 4b. The airfoil is equipped with a total of 8 bimorphs to actuate the trailing edge of the prototype. Each

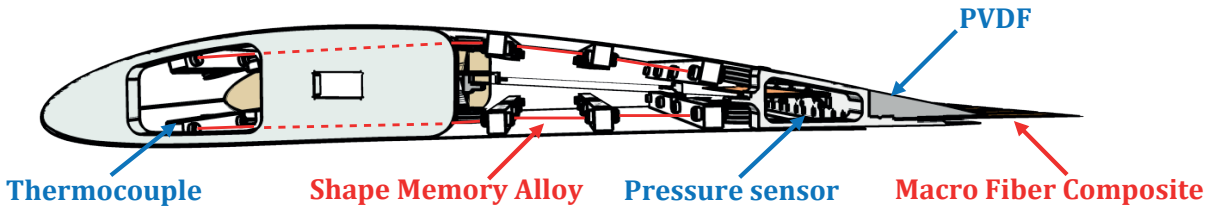

Figure 3: Side view of te mecanism

of these bimorphs can be activated independently and in future application can also provide a feedback as a sensor.

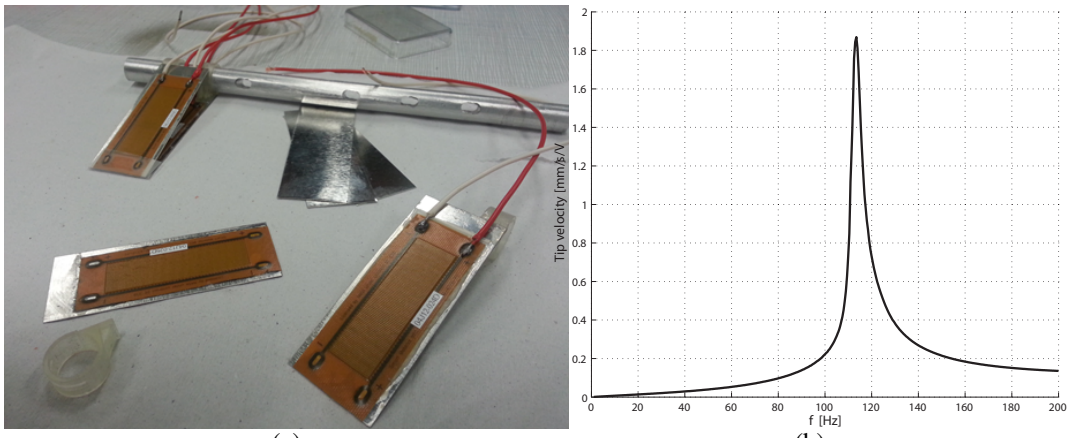

(a) (b)

Figure 4: MFC actuators (a) bonded on both sides of $0.3mm$ steel substrate (b) frequency response

SMAs are continuously distributed under the surface of the structure. Two wires of $90\,\mathrm{cm}$ are used to activate upper and lower surface of the wing respectively. Silicon tubes insulate all SMA wires. This allows both for faster heating and active cooling. In contrast to previous studies both the intrados and extrados of the airfoil are made out of aluminium. While this decision requires the use of a compliant mechanism (illustrated in the trailing edge of the airfoil shown in Figure 3) in order to compensate for the length difference between the actuated and unactuated surfaces it also further approaches industrial demands.

3 Experimental setup

The experiments were conducted in the wind tunnel S4 of IMFT. The dimensions of the test section are $670 \times 715\,mm$. The prototype is mounted on the transversal axis of the wind tunnel with an angle of inclination $-10°$ (descending configuration). The air flow is constant and directed along the x-axis. The upstream turbulence intensity is $0.1\,\%$. Investigations were performed at ambient temperature ($22°C$). In order to measure velocity field by TRPIV, smoke particles are seeded in the air flow by a commercial smoke engine. This smoke engine is put in the upstream convergent part of the wind tunnel.

The upstream velocity field is $8\,m/s$. The chord length is $42.5\,cm$. Hence, the Reynolds number is $218,000$. Figure 5 illustrates the experimental setup. A High speed camera (Phantom v1210) is placed to capture the particle displacements in the flow field at the end of the trailing edge of the structure. The camera is equipped with a $105\,\mathrm{mm}$ Nikon lens. The optical depth of

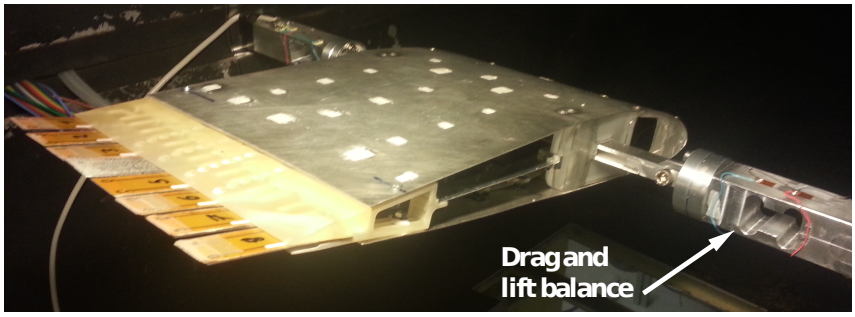

Figure 5: Wind tunel experimental setup

field is focussed on the illuminated laser sheet which corresponds to the *x*-*y* plane. The laser pulsations are generated by a two cavities Nd:YLF ($527\,nm$) laser (Quantronix, Darwin Duo). Using sheet optics a laser sheet is generated in the *x*-*y* plane and focalised on the investigation area. An additional mirror reflects the generated laser sheet so that the laser sheet intersects with the midsection of the structure. The thickness of the laser sheet is $1.5\,mm$.

In this work, the smoke particles diameter distribution is centered near $3.4\,\mu m$. Particle images

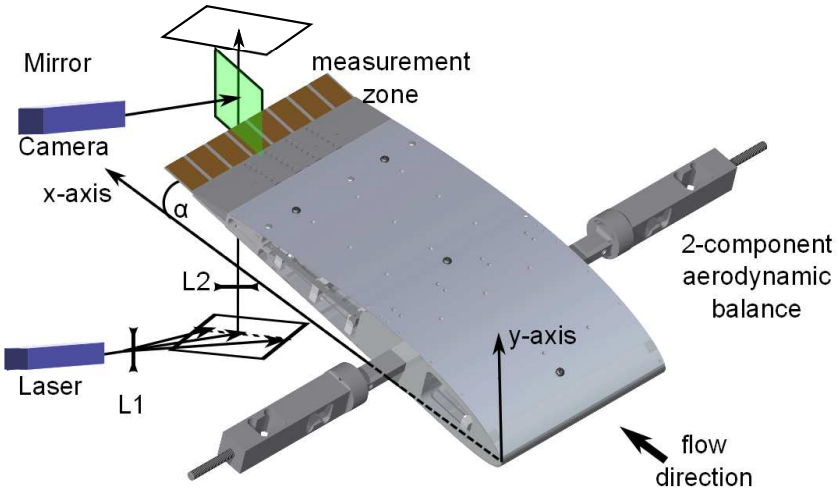

Figure 6: PIV optical set up

are recorded during the duration of the experiment using a digital camera. Each image is divided in "interrogation windows". The interrogation window size is $16 \times 16\,px^2$ (px being Pixel) which corresponds to $2.3 \times 2.3\,\text{mm}^2$, with an overlap of 50%. The most probable displacement of the particles between consecutive images and for a given interrogation window is obtained from the cross-correlation plane of consecutive images. Finally, the particle velocities in the laser sheet are simultaneously calculated from the value of the most probable displacement (depending on the size of the correlation peak) in a given interrogation window and the time delay between two laser pulses. The particle displacement during the bending displacement of the trailing edge flap at $30\,\text{Hz}$, $60\,\text{Hz}$ and $90\,\text{Hz}$ reflects the resulting velocity according to the deflected trailing edge position as the Stokes number (S_k) is much smaller than one ($S_k = \frac{\rho_p d_p^2 U_\infty}{18\mu\delta_c} = 10e-3$, where μ is the dynamic viscosity of the fluid, ρ_p is the density of the smoke particles and δ_c is the characteristic length). This, as suggested by [10] and [20], indicates that the particles follow the motion of the fluid. In order to evaluate the macroscopic effects of the large amplitude morphing on the airflow an aerodynamic balance was added to the

experiment. Boundary sidewalls and profiled hulls isolate balance system from the airflow.A pressure sensor (Kulite XCQ-093 350 mBar) is also integrated into the prototype to evaluate locale pressure around the trailing edge.

4 Experimental results

The experimental results are split in two parts, in a first part the effects of the high-frequent actuation on the flow are analyzed by means of time-averaged Reynolds stress tensors.

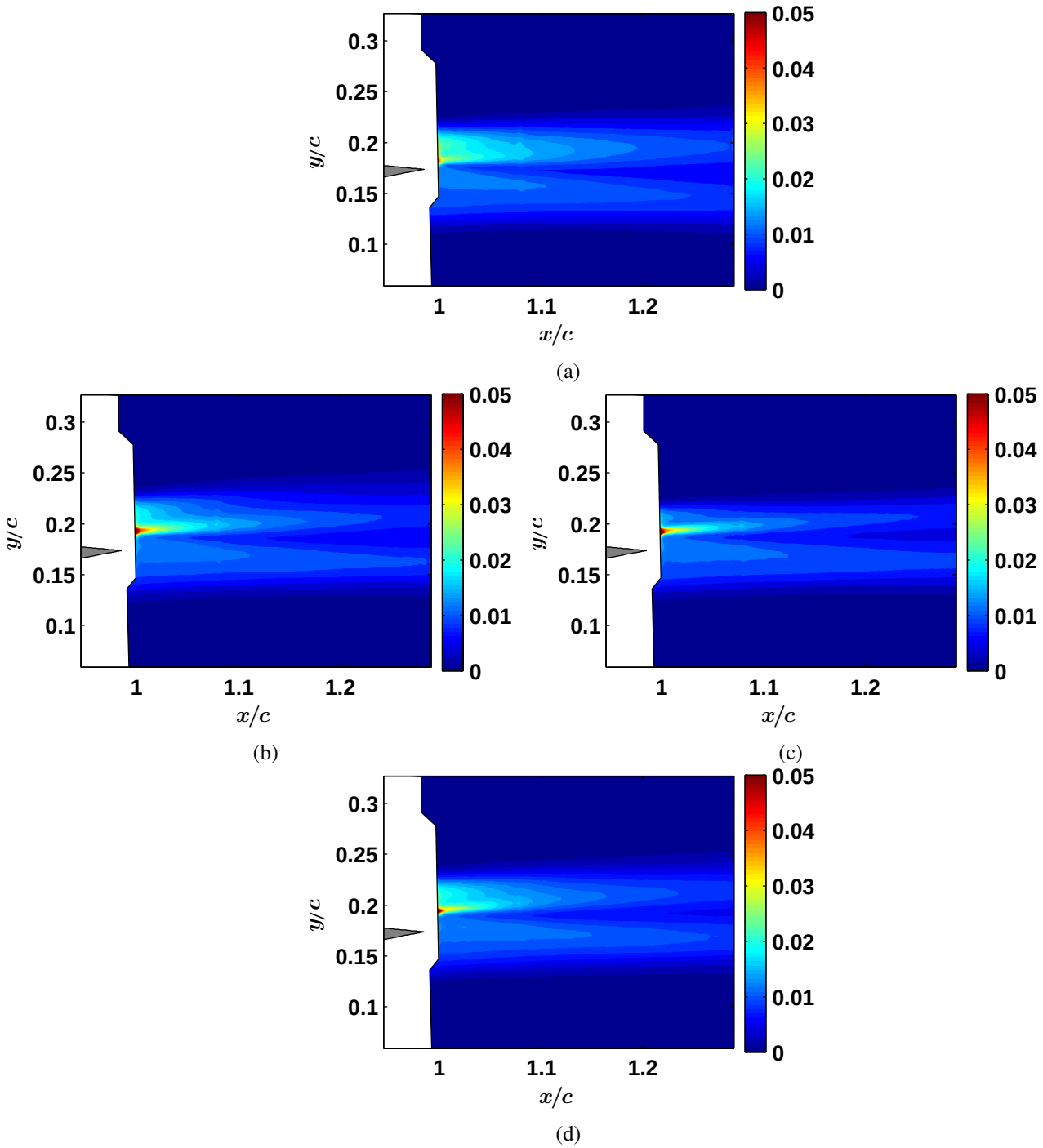

Figure 7: Comparison of $\overline{u^2}$ for (a) 0 Hz,(b) 30 Hz, (c) 60 Hz and (d) 90 Hz

Figures 7,8 and 9 show the time-averaged Reynolds stress fields of the $\overline{u^2}/U_\infty^2$,$\overline{v^2}/U_\infty^2$ and $\overline{uv}/U_\infty^2$ components. The maximum $\overline{u^2}/U_\infty^2$ stress occurs in the shear layer past the trailing edge of the piezoelectric actuated flap. As the actuation frequency increases, the size of the shear layer is reduced which in turn leads to a reduction of the maximum Reynolds stress past the trailing edge of the prototype. This reduction of the shear layer is maximized at 60 Hz.

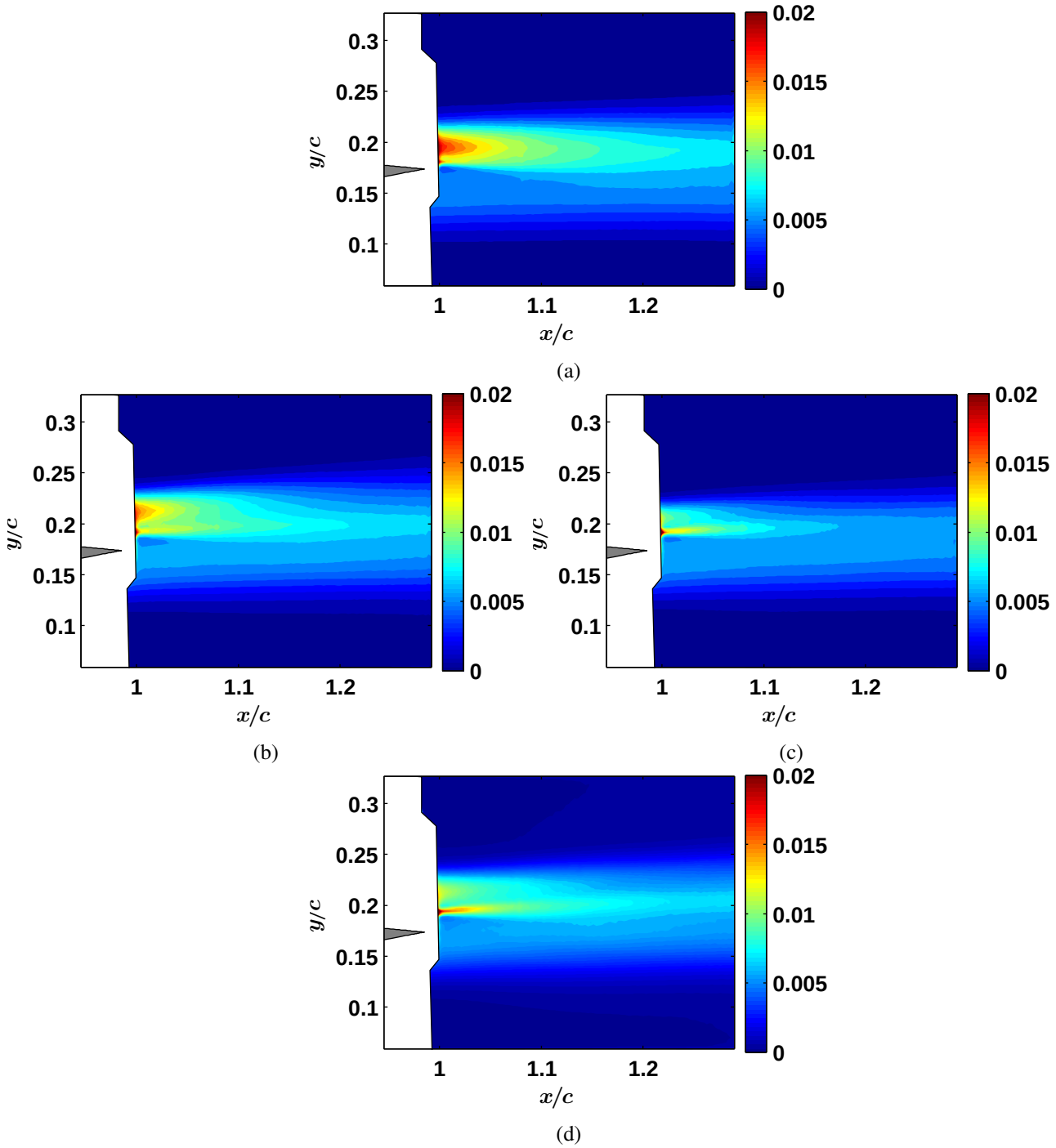

Figure 8: Comparison of $\overline{v^2}$ for (a) 0 Hz,(b) 30 Hz, (c) 60 Hz and (d) 90 Hz

Similarly to the $\overline{u^2}$ Reynolds stress field the $\overline{v^2}/U_\infty^2$ field also experiences a reduction of the maximum Reynolds stress past the trailing edge of the actuated flap. Once again this reduction increases with increasing actuation frequency and is especially evident when comparing the

unactivated "static" case to the actuation at 60 Hz (compare Figures 8a and 8c). The reduction of the $\overline{v^2}$ Reynolds stress field is even more apparent as the flaps deformation is primarily in vertical direction. Once again the maximum reduction of the $\overline{v^2}$ component of the Reynolds stresses can be observed at 60 Hz.

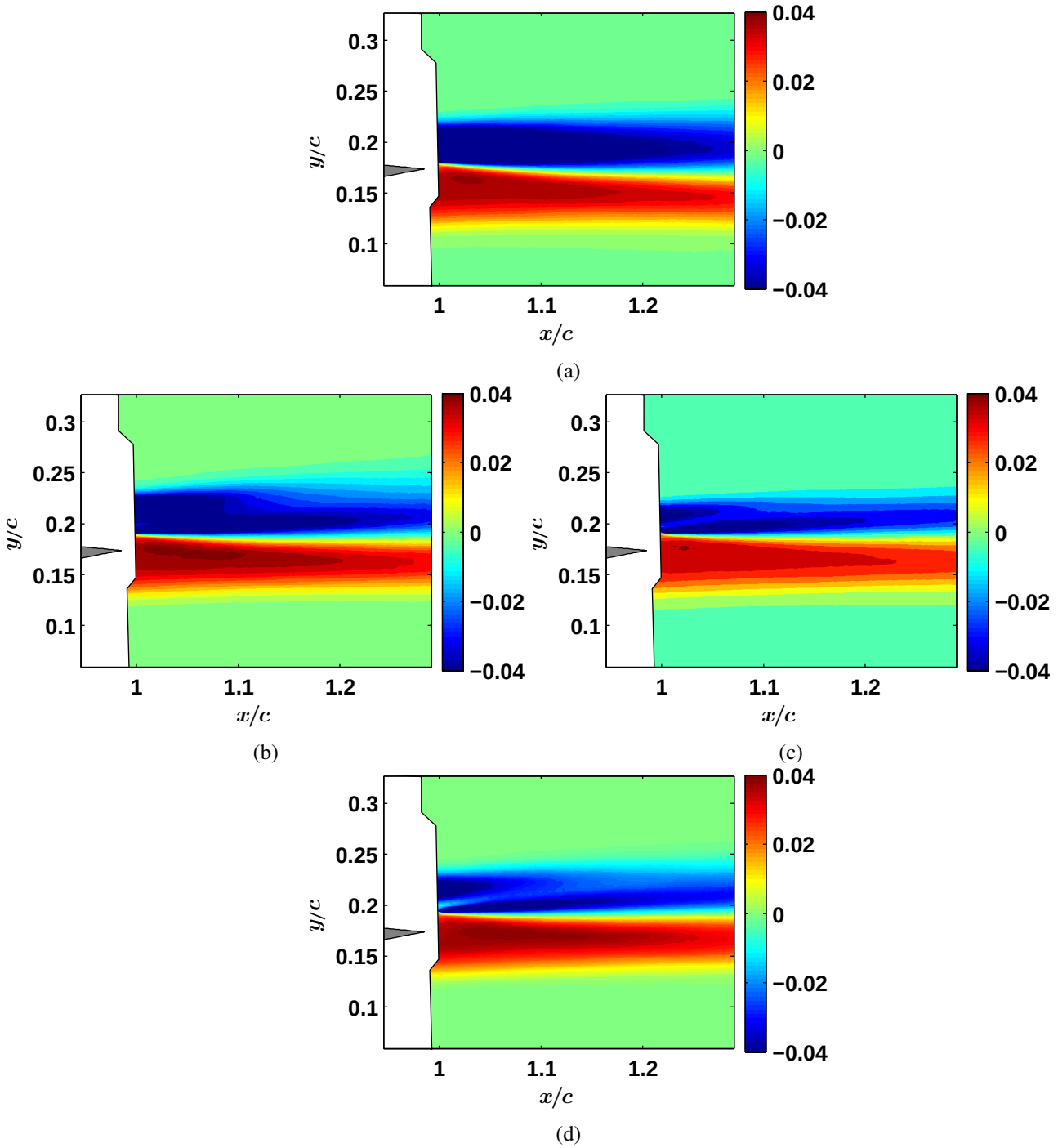

Figure 9: Comparison of $\overline{uv}$ for (a) 0 Hz,(b) 30 Hz, (c) 60 Hz and (d) 90 Hz

The shear-stress components $\overline{uv}/U_\infty^2$ displayed in Figures 9a-9d show a wake similar to a normal wake [6]. As both the $\overline{u^2}$ and $\overline{v^2}$ Reynolds stress tensor components decrease in magnitude with increasing actuation frequency it is reasonable to assume that a similar reduction can also be observed in the shear stress component. This reduction is shown in Figure 9. As the

actuation frequency increases it can be seen that both the upper and the lower wake decrease in size up to an actuation frequency of 60 Hz.

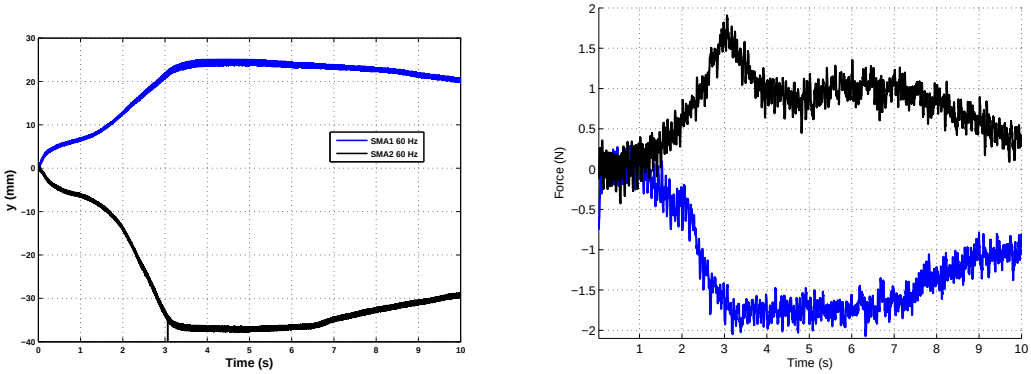

(a) (b)

Figure 10: (a) Trailing edge position vs. time and (b) Lift variation vs. time

The trailing edge position was tracked during the SMA actuation using the data provided by the raw PIV images. The result of this tracking for both the upward and downward deflection of the airfoil is shown Figure 10a. For an angle of attack of $-10°$ with a current of 8 A applied in the SMAs it takes 3 s to reach 30 mm upward or 40 mm downward deflection respectively. The position is held while the systems cools down. As can be seen by comparing Figure 10b to Figure 10a a good correspondance exists between the deflection of the trailing edge of the airfoil and lift force variations. The black curve shows how the y-coordinate of the trailing edge decrease while the wing is changing its camber. The black curve in Figure 10b shows how the lift force is correspondingly increasing. The opposite variation can be observed for the reverse actuation. Hence, it is possible to increase or decrease significantly the lift of the structure with this hybrid morphing system while at the same time acting on the fluctuating velocities.

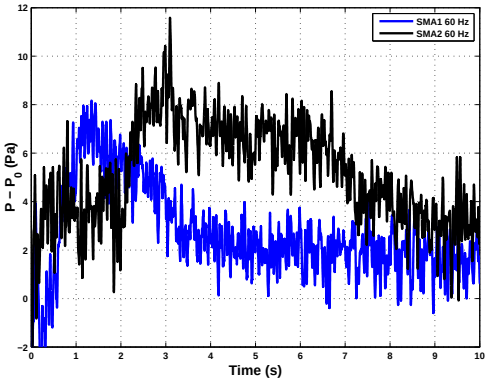

Figure 11: Pressure variation Vs time

The in-situ pressure measurement whose variation over time is shown in Figure 11 shows a good correspondance with the macroscopic lift measurement. This possibly allows to create a simple control loop using the local pressure measurement.

5 Conclusion

The goal of this study was to show the effect of a hybridization of high frequency piezoelectric and low frequency SMA actuation mechanism integrated in an airfoil prototype on the flow. The design of the hybrid prototype was illustrated and a new bimorph MFC actuation mechanism was detailed. Using this prototype it was shown, that the energy induced via the high frequency actuation has a considerable impact on the shear-layer vortex structures. The actuation frequency of the piezoelectric actuation mechanism can clearly be identified in the variations of the local velocity fields. As shown in Section 4 the high-frequent actuation of the trailing edge reduces both the axial component of the Reynolds stress tensor $\overline{u^2}/U_\infty^2$ as well as the transverse component $\overline{v^2}/V_\infty^2$. By exploiting this effect it might be possible to attenuate the high-frequent Kelvin-Helmholtz vortices which are a major source for noise and drag. Furthermore this study confirmed previous observations [21] that an optimum open-loop configuration appear to be close to a frequency of 60 Hz by comparing the Reynolds stress fields.

To the authors knowledge, the use of a hybrid system associating different kinds of electroactive materials is an originality in the state of the art. The feasability of the hybridation under aerdynamic loads at a Reynolds number of $218,000$ has been demonstrated in this article for both a low-frequent large amplitude actuation as well as a high-frequent low amplitude actuation.

Acknowledgements

The authors would like to thank D. Harribey from LAPLACE as well as C. Korbuly from IMFT for their help and support in realizing the present work.

References

[1] S Barbarino, R Pecora, L Lecce, A Concilio, S Ameduri, and E Calvi. A novel SMA-based concept for airfoil structural morphing. *Journal of materials engineering and performance*, 18(5):696–705, 2009.

[2] A Baz, T Chen, and J Ro. Shape control of NITINOL-reinforced composite beams. *Composites Part B: Engineering*, 31(8):631–642, 2000.

[3] Onur Bilgen and Michael I Friswell. Piezoceramic composite actuators for a solid-state variable-camber wing. *Journal of Intelligent Material Systems and Structures*, 25(7):806–817, 2014.

[4] Onur Bilgen, Michael I Friswell, and Mohammed Taqiuddin. Coupled modeling and optimization of piezocomposite wings. In *ASME 2013 Conference on Smart Materials, Adaptive Structures and Intelligent Systems*, pages V002T06A027–V002T06A027. American Society of Mechanical Engineers, 2013.

[5] Onur Bilgen, Drew Landman, and Michael I Friswell. Low reynolds number behavior of a solid-state piezocomposite variable-camber wing. *AIAA Paper*, 1515:8–11, 2013.

[6] Yude Chen, Claude G. Matalanis, and John K. Eaton. High resolution PIV measurements around a model turbine blade trailing edge film-cooling breakout. *Experiments in Fluids*, 44(2):199–209, 2008.

[7] Maxime Chinaud, Jean-François Rouchon, Eric Duhayon, Johannes Scheller, Sebastien Cazin, Moise Marchal, and Marianna Braza. Trailing-edge dynamics and morphing of a deformable flat plate at high reynolds number by time-resolved PIV. *Journal of Fluids and Structures*, (0):–, 2014. ISSN 0889-9746. doi: http://dx.doi.org/10.1016/j.jfluidstructs.2014.02.007. URL http://www.sciencedirect.com/science/article/pii/S0889974614000231.

[8] E. Deri, M. Braza, E. Cid, S. Cazin, D. Michaelis, and C. Degouet. Investigation of the three-dimensional turbulent near-wake structure past a flat plate by tomographic {PIV} at high reynolds number. *Journal of Fluids and Structures*, (0):–, 2013. ISSN 0889-9746. doi: 10.1016/j.jfluidstructs.2012.11.005. URL http://www.sciencedirect.com/science/article/pii/S0889974612002095.

[9] TW Duerig and AR Pelton. TiNi Shape Memory Alloys. In Rodney F Boyer and EW Collings, editors, *Materials properties handbook: titanium alloys*, pages 1035–1048. ASM International, 1994.

[10] Sheldon I Green. *Fluid Vortices: Fluid Mechanics and Its Applications*, volume 30. Springer, 1995.

[11] Khoo Hock Hee. Designing morphing airfoils for improving the aerodynamic characteristics. 2012.

[12] T.O. Ikeda. *Fundamentals of piezoelectricity*. Oxford University Press, 1990.

[13] Chao-Chieh Lan and Chen-Hsien Fan. An accurate self-sensing method for the control of shape memory alloy actuated flexures. *Sensors and Actuators A: Physical*, 163(1): 323–332, 2010.

[14] Justin Edward Manzo. *Analysis and design of a hyper-elliptical cambered span morphing aircraft wing*. PhD thesis, Cornell University, 2006.

[15] David Munday and Jamey Jacob. Active control of separation on a wing with oscillating camber. *Journal of aircraft*, 39(1):187–189, 2002.

[16] Narcis Ursache, Tomas Melin, Askin Isikveren, and Mike Friswell. Morphing Winglets for Aircraft Multi-Phase Improvement. In *7th AIAA ATIO Conf, 2nd CEIAT Int'l Conf on Innov & Integr in Aero Sciences,17th LTA Systems Tech Conf; followed by 2nd TEOS Forum*, Aviation Technology, Integration, and Operations (ATIO) Conferences. American Institute of Aeronautics and Astronautics, September 2007. URL http://dx.doi.org/10.2514/6.2007-7813.

[17] O Ohanian III, Christopher Hickling, Brandon Stiltner, Etan D Karni, Kevin B Kochersberger, Troy Probst, Paul A Gelhausen, and Aaron P Blain. Piezoelectric morphing versus servo-actuated mav control surfaces. *AIAA Paper*, 1512:23–26, 2012.

[18] Matteo Orazi, Davide Lasagna, and Gaetano Iuso. Circular cylinder drag reduction using piezoelectric actuators. *ADVANCES IN AIRCRAFT AND SPACECRAFT SCIENCE*, 1(1): 27–41, 2013.

[19] J Ro and A Baz. Nitinol-reinforced plates: part i. Thermal characteristics. *Composites Engineering*, 5(1):61–75, 1995.

[20] M Samimy and SK Lele. Motion of particles with inertia in a compressible free shear layer. *Physics of Fluids A: Fluid Dynamics (1989-1993)*, 3(8):1915–1923, 1991.

[21] Johannes Scheller, Maxime Chinaud, Jean-François Rouchon, Eric Duhayon, Sebastien Cazin, Moise Marchal, and Marianna Braza. Trailing-edge dynamics of a morphing NACA0012 aileron at high reynolds number by high-speed PIV. *Journal of Fluids and Structures*, (0):–, 2015. ISSN 0889-9746. doi: http://dx.doi.org/10.1016/j.jfluidstructs.2014.12.012. URL http://www.sciencedirect.com/science/article/pii/S0889974615000158.

[22] W Wilkie, J High, and J Bockman. Reliability testing of nasa piezocomposite actuators. 2002.

[23] R Brett Williams, Gyuhae Park, Daniel J Inman, and W Keats Wilkie. An overview of composite actuators with piezoceramic fibers. *Proceeding of IMAC XX*, pages 4–7, 2002.